J Nanostruct 13(4): 1203-1212, Autumn 2023

RESEARCH PAPER

SnO_2 Nanoparticles: Synthesis, Characterization and Their Applications in Removing Drugs from Aqueous Solutions

Hiba Ali Hamzah [1], *Aula M. Al Hindawi* [1]*, *Fouad Fadhil Al-Qaim* [2]

[1] *Department of Chemistry, College of Education for Pure Science, University of Kerbala, Karbala, Iraq*

[2] *Department of Chemistry, College of Sciences for Women, University of Babylon. Hilla, Iraq*

ARTICLE INFO

Article History:
Received 13 June 2023
Accepted 28 September 2023
Published 01 October 2023

Keywords:
Adsorption
Mefenamic acid
SnO_2 nanoparticles

ABSTRACT

SnO_2 nanoparticles have been formed using chemical precipitating method and the resulting particles were then investigated by FESEM (field emission scanning electron microscopy), TEM (transmission electron microscopy), and Fourier-transform infrared spectroscopy (FT-IR).The crystal structure and the grain size were deduced from X-ray diffraction pattern. The band gap energy was calculated from UV-Vis spectrum and it was 3.7 eV, this redshift comparing to bulk SnO_2 could attributed to the quantum effect. The adsorption behavior of SnO_2 Nano crystals was tested with mefenamic acid (MFA) in aqueous solutions. Different certain parameters as pH, MFA concentration, temperature, studying time and adsorbent dosage to determine the best adsorption conditions. It was found that the maximum removal efficiency is 92.6% when the concentration of MFA and dosage of SnO_2 were 30 mg/L and 0.6 g, respectively, within 80 minutes. The MFA adsorption mechanism is consistent with the Freundlich isotherm models.

How to cite this article
Hamzah H., Al Hindawi A., Al-Qaim F. SnO_2 Nanoparticles: Synthesis, Characterization and Their Applications in Removing Drugs from Aqueous Solutions. J Nanostruct, 2023; 13(4):1203-1212. DOI: 10.22052/JNS.2023.04.028

INTRODUCTION

Residues from pharmaceuticals have been considered a major problem affecting the environment and living organisms especially antibiotics and steroids which cause resistance in natural bacteria [1]. Many techniques have recently been proposed and used for removing these pharmaceuticals from wastewater such as activated sludge, osmosis, zonation and membrane bioreactor system. Although such techniques have been used to date, they showed poor removal efficiencies for some pharmaceutical compounds [2, 3]. Physiochemical techniques such as adsorption have shown high efficiency in removing pharmaceutical compounds. Mefenamic acid [*N*-(2, 3-xylyl) anthracitic acid] is one of those pharmaceutical compounds that can cause serious problems to the environment if it is not being treated [4]. Different adsorbents have been utilized for adsorbing mefenamic acid (MFA) from water sources such as activated carbon, which showed a maximum removal efficiency of 60% after 120 minutes when combined with ultraviolet radiation [5]. According to Rodrigo's team, 100% and 96% of MFA were removed from wastewater when activated carbon and red mud, respectively, were used as adsorbents before oxidation with chlorine [6]. In 2020, a novel polyurea formaldehyde with bentonite clay composite was utilized as an adsorbent for removing MFA. The results show

* *Corresponding Author Email: aulamahdi@yahoo.com*

that this adsorption is physical in nature and the adsorption potential is 16 mg\g at 47°C and pH of 1.5. Recently, semiconductor nanostructures have been reported as good adsorbents for removing dyes and pharmaceutical compounds from water source [4, 7, 8]. Among these materials, Tin dioxide (SnO_2) has been studied extensively and used in various fields such as solid-state sensors, catalysts, transparent conductors, Li-batteries. SnO_2 is an n-type semiconductor that has a wide band gap (3.6 eV) which activated only UV irradiation [9, 10]. This activity is restricted by the recombination of the charge carriers (electrons and holes). Extending the absorption of SnO_2 to the visible region requires narrowing the band gap, which can achieve by doping with non-metallic elements. This project aims to synthesize and use SnO_2 nanoparticles, as an adsorbent, for the first time, to remove MFA from wastewater. The impact of SnO_2 dose, contact period, pH solution, and temperature was investigated. The adsorption and kinetic parameters were also studied to provide significant information about the adsorption process.

MATERIAL AND METHODS

Materials

Tin oxide pent hydrate ($SnCl_4.5H_2O$) was purchased from CDH and used without any purification. Concentrated ammonia was purchased from Charlie. De-ionized water was used in this project as a solvent.

Preparation of tin oxide nanoparticles (SnO_2 NPS)

To Prepare SnO_2 nanoparticles, 0.1752 g of tin (IV) chloride pentahydrate ($SnCl_4.5H_2O$) was dissolved in 50 mL of deionized water and stirred for 15 minutes. Thereafter, ammonia solution (25%) was added drop wise to the above aqueous solution under continuous stirring. This was carried out until the solution pH reached 8 and the white precipitate appeared. Deionized water was used to wash the precipitate (three times) to get rid of unwanted materials, in particular, chloride ions. To separate the precipitate, a 4000 rpm centrifuge was utilized for 15 minutes. The sample was dried in a drying oven for 24 hours at 100°C before annealing at 600°C.

Adsorption Studies

The stock solution of MFA was prepared by dissolving 1 g of MFA in 1000 mL of deionized water. This solution was then used to prepare standard solutions with different concentrations (30, 40, 50, 60, 90 mg/L). The best concentration of MFA was measured from the calibration curve and it was found to be 30 ppm.

Characterization

Many techniques were utilized to characterize the prepared SnO_2 nanoparticles. X-ray diffract meter (X pert pro-Analytical) was used to study the crystalline structure of the particles, in addition to the crystallite size. Ultraviolet–visible diffuse reflectance (UV-Vis DRS) spectrum was recorded in the range 200- 1000 nm using a 2550-UV spectrophotometer, Shimadzu-Japan. Fourier-transform infrared spectroscopy (FT-IR) (IRAffinity-1S instrument Shimadzu, Japan) was used to examine the functional group that presents on the SnO_2 particles surface. Field emission scanning electron microscope (Zeiss SIGMA VP-FESEM) and transmission electron microscope (JEOL JEM-2100 LaB6) were used to the characterization of the morphology of the particles and to measure the particle size. The presence of elements in the prepared particles was confirmed by Energy dispersive X-ray spectroscopy (EDS). The adsorption behavior of SnO_2 nanoparticles was studied using UV–Vis spectrophotometer (Double Beam-1800, Shimadzu-Japan).

RESULTS AND DISCUSSION

Optical properties

The probable mechanism for the formation of SnO_2 nanoparticles through the chemical precipitation method is that the addition of aqueous ammonia solution to the stannous salt (to make the solution pH 8) led to form hydroxide ions and subsequently form the precipitate of $Sn(OH)_4$. During the annealing process (600 °C), the precipitate was decomposed and SnO_2 nanoparticles formed [11].

$$Sncl_4 + 4NH_4OH \rightarrow Sn(OH)_4 + 4NH_4Cl \quad (1)$$

$$Sn(OH)_4 \rightarrow SnO_2 + 2H_2O \quad (2)$$

UV-Vis Diffuse reflectance spectroscopy was used to study the optical properties of calcined SnO_2 nanoparticles. The SnO_2 nanoparticles' spectrum, which is given in Fig. 1(a), shows a broad intense absorption edge rising at 320 nm.

This broad peak is associated with the presence of a defect on the surface of the particles due to increasing the surface-to-volume area as the particle size approaches the Nano scale levels [12, 13].

The energy band gap of calcined SnO_2 nanoparticles can be estimated from the absorption spectrum using Tauc plot [14].

$$\alpha h\upsilon = C\,(h\upsilon - Eg)^{n} \quad (3)$$

Here, n is the electronic transition which is equal to 0.5, [15] h is the Plank's constant, C is a constant, α is the absorption coefficient, and ν is the frequency of light. By plotting $(\alpha h\nu)^2$ vs photon energy (hν), one can measure the energy band gap by extending the linear part of the spectrum to the photon energy axis (x axis). Tauc plot gives a band gap of 3.7 eV (see Fig. 1(b)) which is larger than that of bulk SnO_2 (3.6 eV). This could be because the quantum confinement phenomenon [16]. It is well known that as the particle size decreases the band gap of semiconductor materials increased, the absorption edge is shifted toward lower wavelengths, and the quantum size effect becomes obvious. Therefore, this finding confirms the formation of SnO_2 at the nanoscale level.

FTIR analysis

FT-IR spectrum of SnO_2 nanoparticles was recorded in the range of 500-4000 cm^{-1}. The sharp peaks centered between 600 and 650 cm^{-1} are assigned to asymmetric and symmetric Sn-O-Sn stretching vibrations which confirm the formation of SnO_2 nanoparticles [12, 17]. The peak centered at 585 cm^{-1} representing the stretching mode of symmetric O-Sn-O (oxide-bridge functional group) [18]. The peak appears at 1441cm^{-1}, suggesting the presence of a Sn-OH bond [19]. The peaks around 2300 to 2400 cm-1 are probably attributed to the presence of CO_2 group It seems from the FTIR spectrum that there are no water molecules adsorb of the prepared particles surface due to the annealing process at 600 °C.

XRD analysis

The phase and the crystal structures of SnO_2 nanoparticles were studied using XRD. It is clear from Fig. 3 that the prepared SnO_2 nanoparticles have a polycrystalline structure and the diffraction peaks can be assigned to tetragonal rutile SnO_2 (based on JCPDS card No. 41-1445) [20] . This finding is quite similar to previous works [21, 22]. No Phase corresponding to any impurity can be detected in XRD pattern. The grain size of the prepared sample was calculated using Debye Scherer equation:

$$D = K\lambda/\beta\cos\theta \quad (4)$$

Where β is the complete width at half maximum and D is the average crystallite size "in radians",

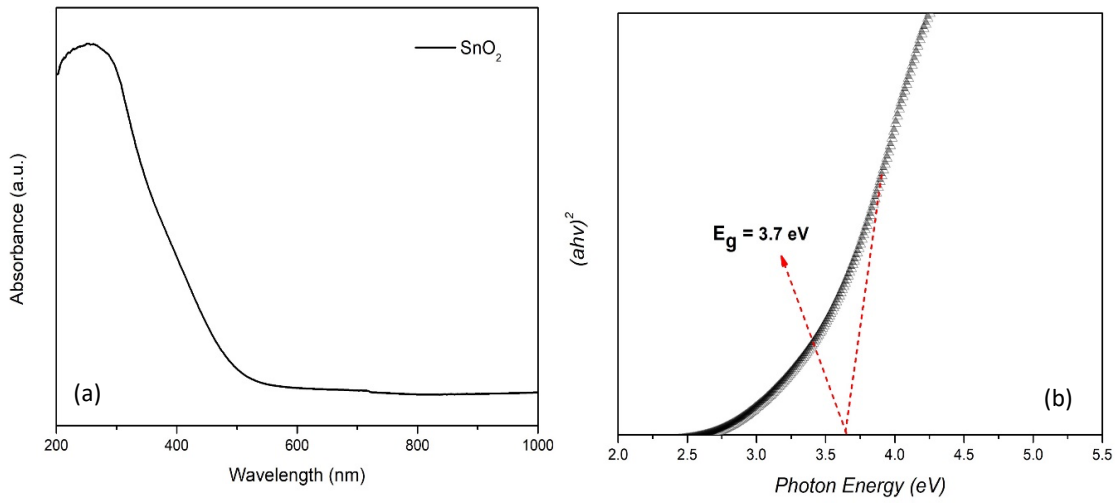

Fig. 1. UV-DRS spectrum of SnO_2 particles formed at pH 8 and annealed at 600 °C (a), the band gap energy estimated from tauc formula (b).

K is the shape factor 0.9, λ is the wavelength of X-ray (0.154 nm), and theta is the Bragg's angle "in radians". The average crystallite size was found to be around 14.4 nm. The average distance between lattice planes was 0.18 nm.

Morphological and EDX Analysis

The surface morphology of SnO_2 NPS was examined using electron microscopy. Fig. 4 (a) shows that the as-prepared SnO_2 nanoparticles have spherical shapes and some of them are clustered

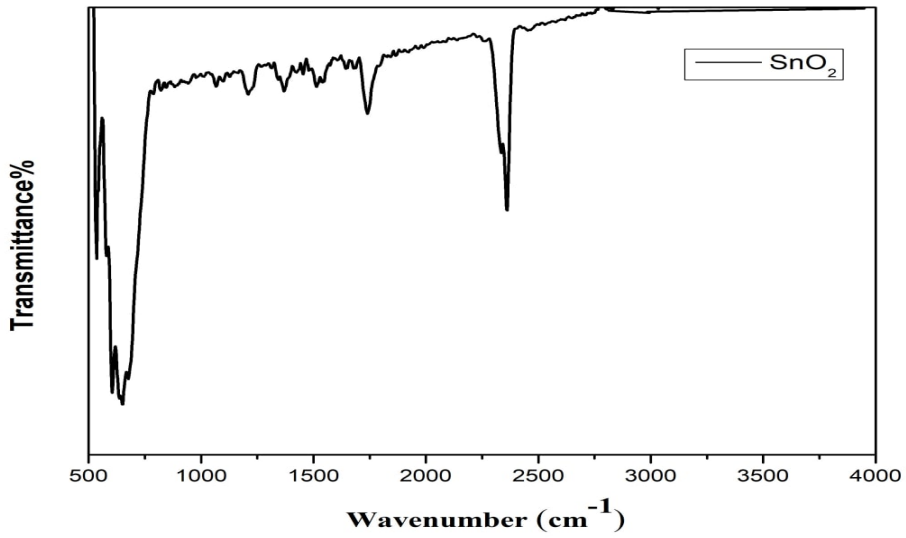

Fig. 2. FTIR spectrum for SnO_2 nanoparticles formed from chemical precipitation method.

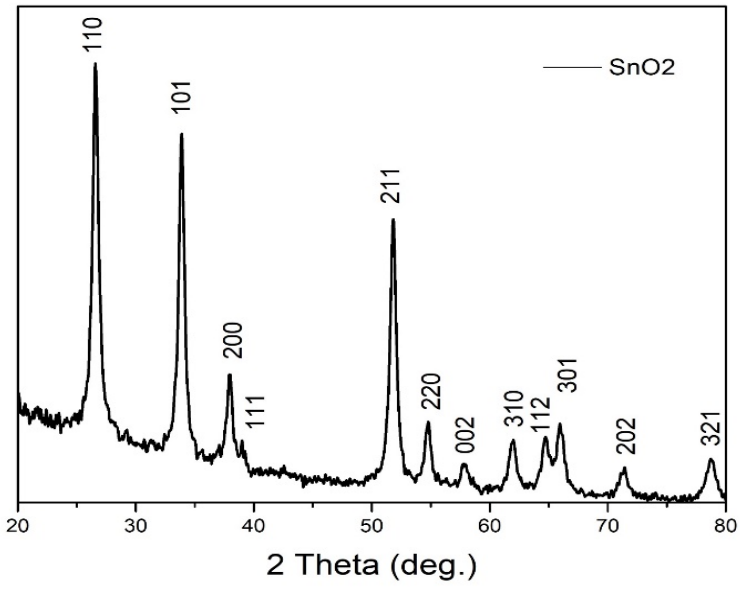

Fig. 3. XRD pattern of synthesized SnO_2 nanoparticles calcined at 600 °C

together. The size of synthesized particles was measured using the image J software [23, 24] and the average size was found to be ~20 nm. The TEM image in Fig. 3(b) shows that SnO_2 nanoparticles are uniform and they almost aggregate with each other. Fig. 3(c) shows the elemental analysis of SnO_2 nanoparticles and it is revealed that the prepared particles have Sn (95.1%) and O (94.9%) elements in their composition. It is worth to mentions that the appearance of the Au element peak in the EDS graph is referred to the coverage process of the sample with gold atoms during the EDS preparation sample [25, 26].

Adsorption of MFA by SnO_2

The impact of adsorption time

To study the effect of adsorption time, five solutions of MFA were prepared with different concentrations (30, 40, 50, 60, and 90 mg/L) from the stock solution and 0.6 mg of adsorbents (SnO_2 nanoparticles) was added to each flask. The flasks were placed on a shaker for 80 min at 298 K. Samples were analyzed at different time intervals (10, 20, 30, 40, 50, 60, 70, 80, 90, and 100

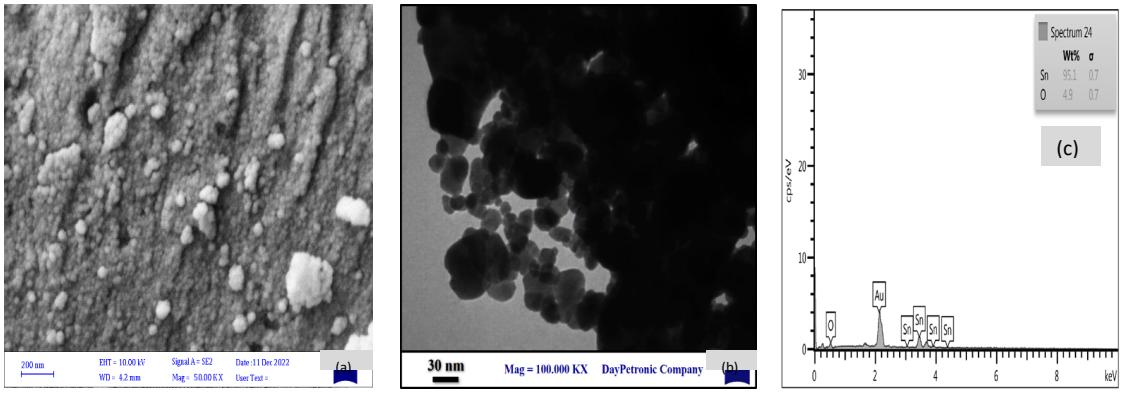

Fig. 4. FESEM image of SnO_2 particles (a), TEM image of synthesized SnO_2 nanocrystals, and (c) EDS graph.

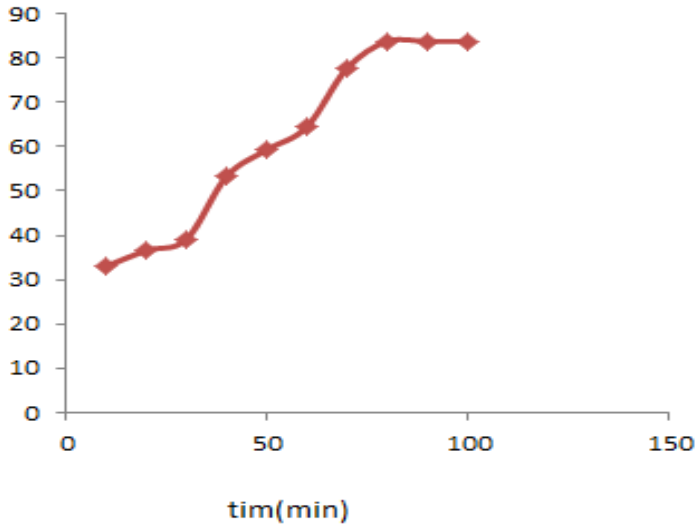

Fig. 5. Contact time's impact on the removal efficiency of MAF at pH 6 and Temperature of 298 K .

minutes). The adsorbent particles were separated using centrifuge (8000 rpm) for 15 minutes after the predetermined amount of time. The maximum absorbance for mefenamic acid was observed at 284 nm using a UV-Vis spectrophotometer, the clear supernatant was examined both before and after adsorption. Calculations were made for the removal effectiveness and adsorption capacity (Q_e) using equations 3 and 4 [4, 27]:

$$R\% = \frac{C_0 - C_e}{C_0} \times 100\% \quad (5)$$

$$Q_e = V(C_0 - C_e)/m \quad (6)$$

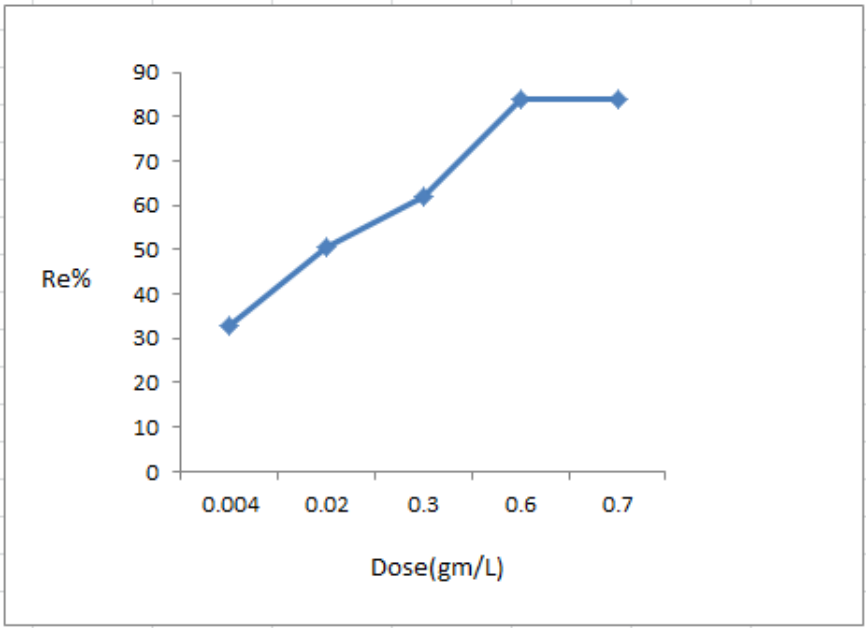

Fig. 6. UV-Vis spectra of tin oxide nanoparticles with MFA as a function of the amount of SnO_2 particles.

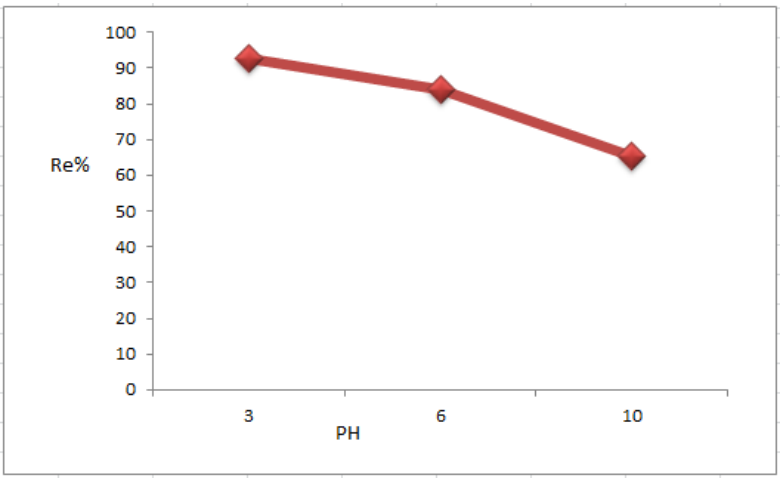

Fig. 7. Effect of pH on the adsorption of MAF on SnO_2 NPs

It is clear from Fig. 5 the removal efficiency increased rapidly during the first 60 minutes, and it became stable at 80, 90, and 100 minutes. This could be because the active sites on the absorbent surfaces will saturate, indicating reaching the apparent equilibrium [28, 29]. Thus, the best efficiency was obtained at the contact time of eighty minutes.

The influence of adsorbent dose

The effect of SnO_2 nanoparticles weight on the adsorption process of MFA was investigated. Fig. 6 shows that when the amount of SnO_2 particles increase the adsorption of the MFA on their surfaces increases too. The removal percentage of MFA increased from 33% to 83.8when the amount of SnO2 particles increased from 0.004 to 0.6 g. The best explanation to this invreament is the presence of large number of active sites and the high surface-to-volume area [30].

The influence of PH

Due to the high surface area of as-synthesized SnO_2 nanoparticles, they consider an excellent

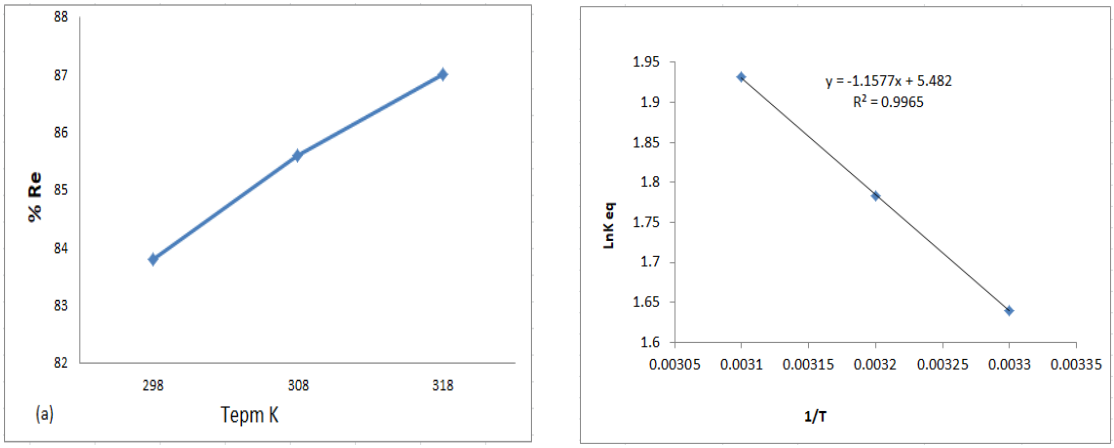

Fig. 8. Influence of temperature on the adsorption behavior of SnO_2 NPs (a) and Van't Hof's equation plots (b)

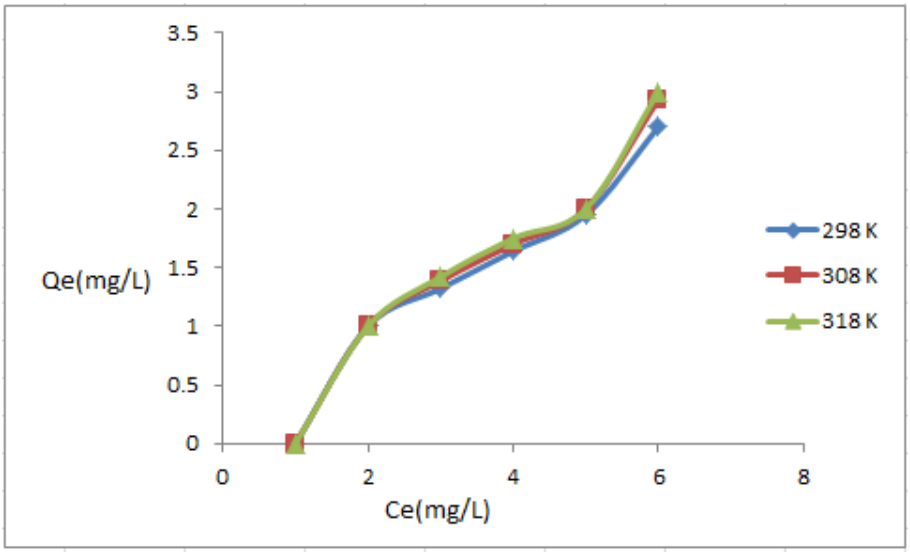

Fig. 9. Adsorption isotherms of MAF

candidate to remove pharmaceutical compounds and dyes from aqueous solutions. PH was varied from (3,6, and 10) by adding either 0.1 M of HCL or 0.1 M NaOH to the solution containing 0.6 g of SnO_2 and 20 mL MFA. The impact of pH on MAF adsorption effectiveness is presented in Fig. 7

The maximum removal efficiency (92.6%) was obtained at pH 3. Due to the positive charged of SnO_2 nanoparticles and negative charge of MFA, electrostatic attractive forces appear leading to enhance the adsorption at acidic pH. Competition between anionic MAF molecules and hydroxyl anions is what causes the reduction in the adsorption capability in an alkaline medium [31].

The effect of temperature on the adsorption process

To determine the temperature required for adsorption, different samples were prepared by mixing 30 ppm of MFA solution with 0.6 g of the prepared tin oxide particles at different temperatures (298, 308, and 318 K). These samples were stirred for 15 minutes at a speed of 140 tr/min and then filtered. The absorbance of the supernatants was then recorded by UV-Vis spectrophotometer. The optimal temperature for adsorbing MFA on the SnO_2 particles surface is 318 K (see Fig. 8(a)) indicating an endothermic adsorption process due to increasing the active adsorption sites and increasing the mobility of mefenamic acid molecules as the temperature increased [32].

Enthalpy change (ΔH°), Gibb's free energy change (ΔG°), and entropy change (ΔS°), which are thermodynamic parameters, were determined by Equations. (3) to (6) [33]. Fig. 8(b) illustrates the effect of temperature on the adsorption behavior of SnO_2 NPs using Van't Hof plotting.

The following equations represent the thermodynamic parameter values:

$$K_{eq} = \frac{Q_{e\times m}}{C_e \times v} \quad (7)$$

$$\Delta G^o = -RT\ln K_c \quad (8)$$

$$\ln K_c = -\frac{\Delta H}{RT} + con \quad (9)$$

$$\Delta S^o = \frac{\Delta H^0 - \Delta G^0}{T} \quad (10)$$

Where, equilibrium adsorption constant is Keq, absolute temperature is K, and ideal gas constant is R. Table 1 reveals that the adsorption procedure is endothermic and spontaneous. The endothermic nature of the adsorption cycle is indicated by the

Table 1. Thermodynamic adsorption parameters of the mefenamic acid over NPs

Adsorbate	Temp. k	ΔG° kj/mol	ΔH° kj/mol	ΔS° J/mol k
MAF	298	-3.966598793	9.6251178×10^{-3}	45.577348
	308	-4.39084882		
	318	-4.879535923		

Table 2. Adsorption isotherm parameters

Temp. (k)	Langmuir isotherm			Freundlich isotherm		
	a (mg/g)	b (mg/L)	R^2 %	n	K_F	R^2 %
298	0.662296	3.711952	0.8256	11.44165	0.747	0.9701
308	0.922424	1.807664	0.7774	10.79914	0.742	0.9679
318	1.019888	2.461841	0.8024	10.71467	0.75	0.9681

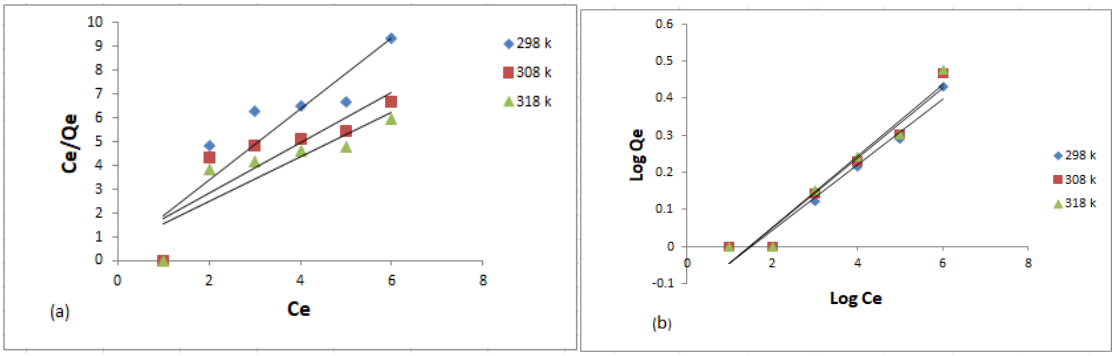

Fig. 10. The linear Langmuir isotherms plot (a) and the Freundlich isotherms (b).

fact that the adsorption capacity starts to rise as the temperature rises. Fig. 9 shows an increase in the MAF's adsorption efficiency from 83.6 to 87% as the temperature increased from 298 to 318 K. In addition, the positive value of ΔS° suggests a high level of species randomization at the MAF adsorbent-adsorbate interactions. Last but not least, the values of H° show that the adsorption mefenamic acid is physisorption [34].

Adsorption isotherms

Isotherms are fundamental prerequisites to the adsorption system design because they allow for the correlation between the residual concentration of MAF in an aqueous solution and adsorption capacity. The Langmuir and Freundlich isotherm models were used to augment by making adjustments to the experimental findings on how temperature affects the adsorption process as shown in Table 2 and Fig. 10.

Langmuir isotherm

The monolayer adsorption described by Langmuir equation has a thickness of one molecule. To analyze the mefenamic acid adsorption process, the Langmuir equation was expressed in its linear form [35]:

$$\frac{C_e}{q_e} = \frac{1}{ab} + \frac{C_e}{a} \qquad (11)$$

a and b are the monolayer coverage-related maximum adsorption capacity (mg/g) and the Langmuir constant (mg/L), respectively. (Fig.10) represents the linear plot of Langmuir isotherm MFA.

Freundlich isotherm

Freundlich equation was used to demonstrate the multilayer adsorption. The following expression provides the Freundlich model [36].

$$\mathrm{Log}Q_e = \mathrm{Log}\, k_f + \frac{1}{n}\,\mathrm{Log}\, Ce \qquad (12)$$

Where n is a variable related to adsorption intensity and Kf (L/mg) is the Freundlich isotherm constant. Fig. 10 depicts the linear plot of the mefenamic acid Freun-Dlich equation (a and b).

CONCLUSION

The current study suggests a new route for the removal of mefenamic acid from aqueous solutions using metal-oxide nanoparticles. The prepared SnO_2 particles have a large optical band gap (3.7 eV) concerning bulk SnO_2 due to the quantum size effect. After research, it was found that 0.6 g of SnO_2 particles are able to adsorb mefenamic acid (MFA) from wastewater with a removal efficiency of ~ 92.6% at pH 3. Based on the thermodynamic functions, the adsorption process of mefenamic acid is endothermic and spontaneous.

CONFLICT OF INTEREST

The authors declare that there is no conflict of interests regarding the publication of this manuscript.

REFERENCES

1. Ternes TA, Hirsch R, Mueller J, Haberer K. Methods for the determination of neutral drugs as well as betablockers and β 2 -sympathomimetics in aqueous matrices using GC/MS and LC/MS/MS. Fresenius J Anal Chem. 1998;362(3):329-340.
2. Rodríguez-Serin H, Gamez-Jara A, De La Cruz-Noriega M, Rojas-Flores S, Rodriguez-Yupanqui M, Gallozzo Cardenas M, Cruz-Monzon J. Literature Review: Evaluation of Drug

Removal Techniques in Municipal and Hospital Wastewater. International journal of environmental research and public health. 2022;19(20):13105.
3. Salim Mahtab M, Haq Farooqi I. An Overview of Occurrence and Removal of Pharmaceuticals from Sewage/Wastewater. Sewage - Recent Advances, New Perspectives and Applications: IntechOpen; 2022.
4. Albo Hay Allah MA, Alshamsi HA. Green synthesis of ZnO NPs using Pontederia crassipes leaf extract: characterization, their adsorption behavior and anti-cancer property. Biomass Conversion and Biorefinery. 2022;14(9):10487-10500.
5. Rivas J, Gimeno O, Encinas A, Beltrán F. Ozonation of the pharmaceutical compound ranitidine: Reactivity and kinetic aspects. Chemosphere. 2009;76(5):651-656.
6. Moruzzi RB, Lima VB, Colombo R, Conceição FT, Lanza MRV. Mefenamic Acid Removal in Water Using Activated Carbon Powder, Red Mud and Oxidation with Chlorine. Quim Nova. 2014.
7. Abed AQ, Hindawi AMA, Alesary HF. Synthesis and characterization of zinc sulfide nanomaterials for removal methylene blue dye from aqueous solution. AIP Conf Proc: AIP Publishing; 2023. p. 020001.
8. Turki ZT, Hindawi AMA, Shiltagh NM. Fabrication and characterization of cadmium sulfide nanoparticles using chemical precipitation method. AIP Conf Proc: AIP Publishing; 2023. p. 030008.
9. Liang X, Wang J, Zhang S, Wang L, Wang W, Li L, et al. Fabrication of uniform Si-incorporated SnO_2 nanoparticles on graphene sheets as advanced anode for Li-ion batteries. Applied Surface Science. 2019;476:28-35.
10. Singh AV, Jahnke T, Xiao Y, Wang S, Yu Y, David H, et al. Peptide-Induced Biomineralization of Tin Oxide (SnO_2) Nanoparticles for Antibacterial Applications. Journal of Nanoscience and Nanotechnology. 2019;19(9):5674-5686.
11. Chakraborty S, Roy M, Saha R. Cost-effective synthesis method of facile environment friendly SnO_2 nanoparticle for efficient photocatalytic degradation of water contaminating compound. Water Sci Technol. 2020;81(3):508-517.
12. Digest Journal of Nanomaterials and Biostructures.
13. Mariammal RN, Ramachandran K, Renganathan B, Sastikumar D. On the enhancement of ethanol sensing by CuO modified SnO2 nanoparticles using fiber-optic sensor. Sensors Actuators B: Chem. 2012;169:199-207.
14. Wooten F, Davis SP. Optical Properties of Solids. American Journal of Physics. 1973;41(7):939-940.
15. Daideche K, Lahmar H, Lerari D, Azizi A. Influence of deposition potential on the electrochemical growth and photocatalysis performance of SnO_2 nanostructures. Inorg Chem Commun. 2023;147:110154.
16. Mohana Priya S, Geetha A, Ramamurthi K. Structural, morphological and optical properties of tin oxide nanoparticles synthesized by sol–gel method adding hydrochloric acid. Journal of Sol-Gel Science and Technology. 2016;78(2):365-372.
17.. Digest Journal of Nanomaterials and Biostructures. 2021;16(2).
18. Akram M, Saleh AT, Ibrahim WAW, Awan AS, Hussain R. Continuous microwave flow synthesis (CMFS) of nano-sized tin oxide: Effect of precursor concentration. Ceram Int. 2016;42(7):8613-8619.
19. Elango G, Kumaran SM, Kumar SS, Muthuraja S, Roopan SM. Green synthesis of SnO_2 nanoparticles and its photocatalytic activity of phenolsulfonphthalein dye. Spectrochimica Acta Part A: Molecular and Biomolecular Spectroscopy. 2015;145:176-180.
20. Anbarasan PM, Priyadharsini CI, Sathiyapriya R, Hariharan V, Parabakaran K, Aroulmoji V. Development of TiO_2 Nanomaterials and Dyes Selection (using DFT) for DSSC Applications –A Stepwise Review. International Journal of Advanced Science and Engineering. 2019;06(02):1326-1350.
21. Characterization of Spray Pyrolysised Nano Tin Disulphide Thin Film. International Journal of Thin Films Science and Technology. 2020;9(1):1-5.
22. Srinivasa Subbarao P, Aparna Y, Chitturi KL. Synthesis and characterization of Ni doped SnO2 nanoparticles by sol-gel method for novel applications. Materials Today: Proceedings. 2020;26:1676-1680.
23. Schneider CA, Rasband WS, Eliceiri KW. NIH Image to ImageJ: 25 years of image analysis. Nat Methods. 2012;9(7):671-675.
24. Mandea V, Marinciu C-M, Şerban G, Ciontu C, Săulescu NN. Genetic and Environmental Effects on Grain Size Uniformity in Winter Wheat. Romanian Agricultural Research. 2022;39:133-138.
25. Chen Z, Fang L, Dong W, Zheng F, Shen M, Wang J. Inverse opal structured Ag/TO2 plasmonic photocatalyst prepared by pulsed current deposition and its enhanced visible light photocatalytic activity. J Mater Chem A. 2014;2(3):824-832.
26. Ju L, Chen Z, Fang L, Dong W, Zheng F, Shen M. Sol–Gel Synthesis and Photo-Fenton-Like Catalytic Activity of $EuFeO_3$ Nanoparticles. J Am Ceram Soc. 2011;94(10):3418-3424.
27. Ahmad MA, Rahman NK. Equilibrium, kinetics and thermodynamic of Remazol Brilliant Orange 3R dye adsorption on coffee husk-based activated carbon. Chem Eng J. 2011;170(1):154-161.
28. Zhu M-X, Lee L, Wang H-H, Wang Z. Removal of an anionic dye by adsorption/precipitation processes using alkaline white mud. J Hazard Mater. 2007;149(3):735-741.
29. Oribayo O, Olaleye OO, Akinyanju AS, Omoloja KO, Williams SO. Coconut shell-based activated carbon as adsorbent for the removal of dye from aqueous solution: equilibrium, kinetics, and thermodynamic studies. Nigerian Journal of Technology. 2021;39(4):1076-1084.
30. Uddin MT, Sultana Y, Islam MA. Nano-sized SnO_2 Photocatalysts: Synthesis, Characterization and Their Application for the Degradation of Methylene Blue Dye. Journal of Scientific Research. 2016;8(3):399-411.
31. Shirzadi A, Nezamzadeh-Ejhieh A. Enhanced photocatalytic activity of supported CuO–ZnO semiconductors towards the photodegradation of mefenamic acid aqueous solution as a semi real sample. J Mol Catal A: Chem. 2016;411:222-229.
32. Osman AM, Hendi AH, Saleh TA. Simultaneous adsorption of dye and toxic metal ions using an interfacially polymerized silica/polyamide nanocomposite: Kinetic and thermodynamic studies. J Mol Liq. 2020;314:113640.
33. Al-Rufaie MM, Alsultani ZTA, Waheed AS. Adsorption kinetics and thermodynamics of Azure C dye from aqueous solution onto activated charcoal. Koroze a ochrana materialu. 2016;60(3):80-85.
34. Arumugam TK, Krishnamoorthy P, Rajagopalan NR, Nanthini S, Vasudevan D. Removal of malachite green from aqueous solutions using a modified chitosan composite. Int J Biol Macromol. 2019;128:655-664.
35. Langmuir I. The Adsorption Of Gases on Plane Surfaces of Glass, Mica And Platinum. Journal of the American Chemical Society. 1918;40(9):1361-1403.
36. Freundlich H. Über die Adsorption in Lösungen. Zeitschrift für Physikalische Chemie. 1907;57U(1):385-470.